


Article

Fracture Parameters Optimization and Field Application in Low-Permeability Sandstone Reservoirs under Fracturing Flooding Conditions

Cong Lu ¹, Li Ma ^{1,*}, Jianchun Guo ^{1,*}, Lin Zhao ², Shiqian Xu ¹, Bugao Chen ³, Yulong Zhou ³, Haoren Yuan ³ and Zhibin Tang ³

¹ State Key Laboratory of Oil and Gas Reservoir Geology and Exploitation, Southwest Petroleum University, Chengdu 610500, China

² CNOOC Research Institute Co., Ltd., Beijing 100029, China

³ Sinopec Shengli Oil Field Luming Oil-Gas Exploration & Development Co., Ltd., Dongying 257000, China

* Correspondence: swpumali177@163.com (L.M.); guojianchun@vip.163.com (J.G.)

Abstract: To solve engineering problems in the production process after fracturing and flooding of low-permeability sandstone reservoirs, such as rapid water-cut rise and low water flooding efficiency, a method for optimizing the fracture parameters of low-permeability sandstone reservoirs under fracturing flooding conditions was proposed. A rock property test experiment was first carried out, the fracturing coefficient was defined, and an evaluation method for the brittleness index of low-permeability sandstone was established to optimize the perforation location of the fracturing reservoir. A productivity numerical model for the two-phase flow of oil–water in matrix–fracture media was established to optimize the fracture morphology under fracturing flooding conditions. The results showed that the quartz content, Young’s modulus, and peak stress mainly affected the fracturing coefficient of rock and are the key indicators for evaluating the brittleness of low-permeability sandstone reservoirs. For production wells in the direction of minimum horizontal principal stress, the swept area of water flooding should be expanded, fracture length should be optimized to 90 m, and fracture conductivity should be 20 D·cm. For fracturing production wells in the direction of maximum horizontal principal stress, the advancing speed of the water injection front should be slowed down to reduce the risk of water channeling in injection-production wells. The optimized fracture length was 80 m, and the fracture conductivity was 25 D·cm. The application of these findings can markedly improve oil production and provide a reference for optimizing the fracture parameters of low-permeability sandstone reservoirs under fracturing flooding conditions.

Keywords: low-permeability sandstone; fracturing flooding; hydraulic fracturing; brittleness evaluation; fracture parameters



Citation: Lu, C.; Ma, L.; Guo, J.; Zhao, L.; Xu, S.; Chen, B.; Zhou, Y.; Yuan, H.; Tang, Z. Fracture Parameters Optimization and Field Application in Low-Permeability Sandstone Reservoirs under Fracturing Flooding Conditions. *Processes* **2023**, *11*, 285. <https://doi.org/10.3390/pr11010285>

Academic Editor: Yidong Cai

Received: 28 December 2022

Revised: 11 January 2023

Accepted: 11 January 2023

Published: 16 January 2023



Copyright: © 2023 by the authors. Licensee MDPI, Basel, Switzerland. This article is an open access article distributed under the terms and conditions of the Creative Commons Attribution (CC BY) license (<https://creativecommons.org/licenses/by/4.0/>).

1. Introduction

With the development of oil and gas exploration and technology, oil and gas development has shifted from conventional reservoirs to unconventional reservoirs that have low permeability and are difficult to produce in China. Hydraulic fracturing is a key technology for the effective production and economic development of unconventional reservoirs [1–3]. Conventional water and chemical flooding can improve reservoir recovery to a certain extent; however, there are still related problems in the development of low-permeability reservoirs [4]. The conventional fracturing process is complex, expensive, has a small scope for fracture control, and the effect of reservoir stimulation is poor. Conventional water flooding has poor hydrodynamic connections, extensive water channeling and flooding, and non-Darcy flow characteristics of fluids, which lead to problems such as “no injection and no production” in low-permeability reservoirs. In conventional chemical flooding, the oil displacement agent adsorbs and remains in the pores of the formation rock, and the

concentration decreases, which leads to a reduction in the oil displacement efficiency [5]. Therefore, “fracture-injection-production” integrated reservoir simulation technology (fracturing flooding) was proposed for the oilfield sites, which perfectly combines hydraulic fracturing technology, conventional water flooding development, and chemical flooding to form a set of continuous development technologies [6].

Since 2000, fracturing flooding technology has been applied and developed in the Daqing and Changqing oilfields, and there are some low-permeability blocks in the Shengli oilfield. The development of this technology mainly involves four stages: matrix imbibition technology for low-permeability reservoirs (2000–2009), fracture–matrix dynamic imbibition technology for fractured low-permeability reservoirs (2010–2014), energy storage fracture network fracturing technology (2015–2016), and energy storage fracturing-imbibition oil recovery technology (2017–present) [7–10]. Based on the operation mode and stimulation mechanism, the fracturing flooding process is divided into two methods: reverse fracturing flooding and forward fracturing flooding [11]. Reverse fracturing flooding involves opening the formation using a low-viscosity fluid instead of a fracturing fluid from the production well and quickly injecting liquid containing an oil-displacing agent through the fracture to increase the reservoir pressure. During the well shut-in process, the flow direction of the wetting phase that is sucked in by the reservoir matrix is opposite to the flow direction of the discharged non-wetting phase, and the reservoir recovery is improved through the enhanced oil–water imbibition displacement between the fracture and matrix. Forward fracturing flooding involves injecting a large amount of liquid containing an oil-displacing agent from an injection well at a pressure that exceeds the formation fracture pressure. Reservoir recovery is improved by increasing the reservoir pressure and oil displacement effect of the oil displacement agent. This study focuses on forward fracturing flooding technology, which has been applied to the Shengli oilfield on a large scale since 2020. More than 40 well group tests have been completed in Bonan, Niuzhuang, and other blocks, and the cumulative water injection is $110 \times 10^4 \text{ m}^3$, with a cumulative increase of 33,000 tons of oil, achieving certain economic benefits [12]. However, this technique also faces two difficulties regarding the optimization of fracture parameters: poor matching of perforation horizons between injection and production wells and unreasonable fracture morphology (fracture length and fracture conductivity), resulting in engineering problems such as rapid water cut rise, low oil displacement efficiency, and short effective production time in some production wells. Therefore, optimizing the perforation location of the well and the fracture parameters of the production well are important methods for improving fracturing flooding technology.

The rock brittleness index is a key parameter for optimizing perforation location [13–16]. Hucka and Das [17] calculated rock brittleness using compressive and tensile strengths through uniaxial compressive strength and Brazilian testing. Later, many scholars used rock mechanical parameters and rock brittle mineral content to characterize rock brittleness and believed that horizon rocks with large brittleness indexes were more prone to fracture and formed a complex fracture network; therefore, the perforation location was optimized according to the brittleness index [18–20]. Presently, there are three types of methods for evaluating rock brittleness: mineral composition, mechanical parameters, and stress–strain parameters [21]. These three parameters are all related to brittleness; however, the fitting degree is not high. Therefore, it is necessary to develop a new method to characterize rock brittleness and improve the accuracy of brittleness prediction.

Optimizing and controlling the hydraulic fracture morphology is the key to the injection-production effect of the well group. Xiao and Guo [22] established a low-permeability heterogeneous geological model for the numerical simulation of hydraulic fracturing. The results show that there is an optimal value for fracture conductivity and fracture length. Xu et al. [23] used the Eclipse software to conduct orthogonal simulations for the fracture network fracturing of low-permeability oil and gas reservoirs to optimize the fracture parameters of horizontal wells. Lei et al. [24] established a non-planar three-dimensional fracture propagation model, proposed a method for the stimulation of low-permeability

oil reservoirs based on the optimal design of fracture-controlled fracturing, and optimized the fracture parameters of horizontal wells. Few scholars have optimized the fracture parameters for low-permeability sandstone reservoirs under the influence of fracturing flooding [25,26]. Engineers at fracturing sites usually operate based on experience and lack theoretical guidance.

In this study, the fracture parameters were optimized from two aspects: perforation location and fracture morphology. First, considering the influence of various factors—such as the mechanical properties, mineral composition, and deformation characteristics of the rock—and using the rock fracturing coefficient as an index, a new method for brittleness evaluation of low-permeability sandstone reservoirs was proposed and the perforation location of the reservoir was optimized accordingly. Furthermore, considering the influence of the oil-displacing agent and hydraulic fractures, a productivity numerical model for the two-phase flow of oil–water in matrix–fracture dual-permeability media was established to optimize fracture morphology under fracturing flooding conditions. Finally, its application in the oil field proved that the technology has good practicability.

2. Perforation Location Optimization Based on Brittleness Evaluation

2.1. Rock Property Testing Experiment

Taking the low-permeability sandstone of the fourth member of the Shahejie formation in the Bohai Bay basin with a burial depth of 2500–3000 m as an example, 13 groups of downhole rock cores were selected for the rock property testing experiment. The stress–strain characteristics, fracture morphology, and mechanical parameters of the core were obtained through triaxial mechanical experiments.

The mineral compositions of the 13 groups of rocks were obtained using whole-rock mineral analysis. The results (Table 1) show that the mineral types of the sandstone in the fourth member of the Shahejie formation include clay minerals, quartz, feldspar, and carbonate minerals, with average contents of 34, 41, 16, and 9%, respectively. The mineral composition distribution of this block was significantly different and exhibited strong heterogeneity.

Table 1. Basic parameters of the core.

Core	Mineral Composition				Mechanical Parameters		Stress–Strain Parameters			
	Case	Clay (%)	Quartz (%)	Feldspar (%)	Carbonate (%)	Poisson's Ratio	Young's Modulus (MPa)	Peak Stress (MPa)	Residual Stress (MPa)	Peak Strain (%)
1	36.1	32.7	21	10.1	0.186	18,905.4	175	95	1.15	1.48
2	7.4	29.2	45	18.5	0.474	17,829	63	38	0.39	0.49
3	7.4	29.2	45	18.5	0.266	10,338.3	49	39	0.42	0.73
4	13.6	30.6	40.3	15.4	0.278	22,125.7	270	175	1.56	1.98
5	15.9	38.7	39.1	6.4	0.24	16,937.5	74	40	0.53	0.6
6	15.9	38.7	39.1	6.4	0.274	12,209.3	82	40	0.9	1.32
7	15.9	38.7	39.1	6.4	0.359	14,529	114	61	0.95	1.18
8	12.6	30	53.4	4	0.26	6951.2	27	16	0.58	0.82
9	12.6	30	53.4	4	0.25	9223.7	35	19	0.51	0.73
10	15.3	30	43.8	10.9	0.239	16,448.8	118	78	0.92	1.24
11	15.3	30	43.8	10.9	0.246	16,617.9	120	82	0.87	1.12
12	27.6	30.7	30.9	10.8	0.058	11,602.3	140	122	2.1	4.2
13	27.6	30.7	30.9	10.8	0.437	8629.6	38	19	0.52	0.63

The rock samples were cut into standard rock pillars (2.5 cm in diameter and 5 cm in length), and triaxial mechanical experiments were conducted on the rock pillars using the RTR-1000 rock mechanics experimenter. The Young's modulus of the sandstone in the fourth member of the Shahejie formation is between 7000 MPa and 28,000 MPa, as shown in Table 1, with an average value of 14,856 MPa; the Poisson's ratio is between 0.06 and 0.474,

with an average value of 0.254. Using the parameters of the triaxial mechanical experiment, the stress–strain curves of the rock pillar at different stress stages were generated, and the peak strain, residual strain, peak stress, and residual stress were calculated. The analysis shows that, under the same confining pressure, there are significant differences in the mechanical parameters, and the overall heterogeneity of the fourth member of the Shahejie formation is strong.

2.2. Fracture Morphology Analysis

The fracture morphology of the rock is important for determining the brittleness of the reservoir rock. A comparative analysis of the rock fracture modes, which was conducted after the experiment, shows that the fracture forms are divided into three types—single shear fractures, split fractures, and complex fractures—as shown in Figure 1.

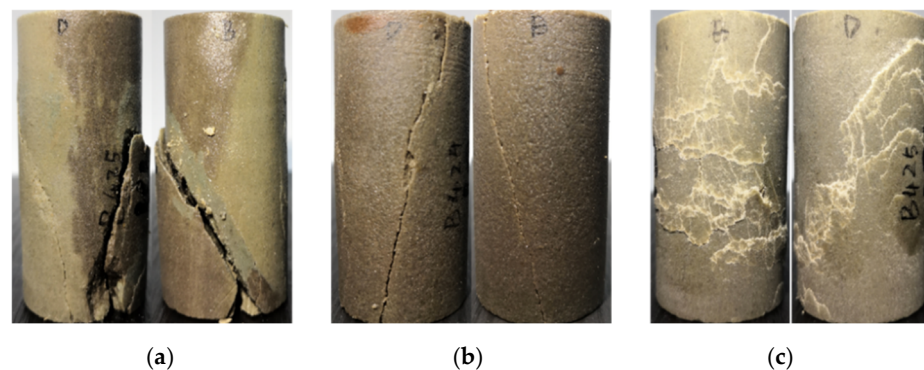


Figure 1. Core fracture morphology. (a) Single shear fractures. (b) Split fractures. (c) Complex fractures.

Many scholars have qualitatively described the characterization of the fracture shape of the core; however, there are few quantitative characterization methods for the fracture mode of low-permeability sandstone. Through classical brittleness index analysis, it was found that there is no direct correlation among rock mechanical parameters, mineral composition, and the three fracture forms of rock [27]; therefore, it is necessary to explore a new brittleness index characterization method.

As shown in Figure 2, the fractal dimension (D) of the core end-face fracture was deduced using box theory [28], and the calculation equation is as follows:

$$D = \frac{C_p - \ln(N)}{\ln(R)} \quad (1)$$

where D is the fractal dimension of the core end-face fracture (dimensionless), R is the side length of the square boxes (cm), N is the number of square boxes containing fractures, and C_p is the proportionality constant.

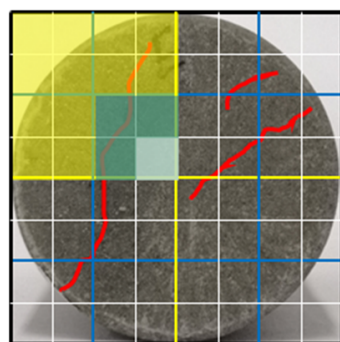


Figure 2. Schematic diagram of the box theory. The red lines represent fractures.

As shown in Figure 3, the fracture morphology on the side of the rock pillar can also characterize the fracture characteristics to a certain extent. Considering the effects of the fractal dimension and the fracture angle of the rock pillar, a rock-fracture complexity coefficient (F_c) is defined. The calculation method is shown in Equation (2), and the calculation results are listed in Table 2.

$$F_c = D \cdot \left(1 - \frac{\alpha}{90}\right) \quad (2)$$

where F_c is the fracturing coefficient (dimensionless) and α is the fracture angle ($^\circ$).

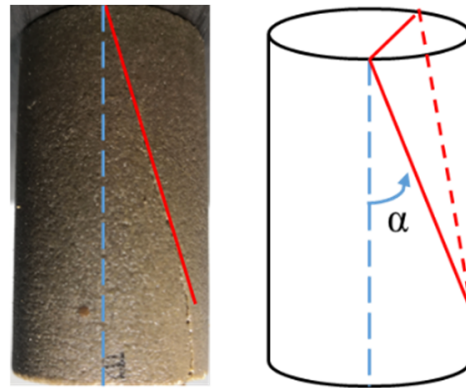


Figure 3. Schematic of the fracture angle on the side of the rock pillar.

Table 2. Fracture morphology parameters.

Core Case	Fracture Morphology	Fractal Dimension	Fracture Angle ($^\circ$)	Fracturing Coefficient
1	split fractures	1.20	5	1.20
2	single shear fractures	1.50	25	1.08
3	single shear fractures	1.36	20	1.06
4	complex fractures	1.96	45	1.24
5	split fractures	1.69	12	1.17
6	split fractures	1.35	12	1.17
7	split fractures	1.94	9	1.08
8	complex fractures	1.44	35	1.20
9	split fractures	1.44	10	1.19
10	complex fractures	1.47	36	1.21
11	split fractures	1.20	4	1.20
12	single shear fractures	1.58	20	1.05
13	complex fractures	1.39	42	1.20

From Equation (2), it can be deduced that the larger the fractal dimension (D) and the smaller the fracture angle (α), the larger the fracturing coefficient (F_c) and the more complex the fracture morphology. As shown in Figure 4, the relationship between the fracturing coefficient and the fracture morphologies of the different cores was compared and analyzed. Cores with fracturing coefficients between 1 and 1.1 showed shear fractures or split fractures, cores with coefficients between 1.1 and 1.2 showed split fractures, and cores with coefficients greater than 1.2 showed complex fractures. Therefore, the core fracturing coefficient had a good correlation with the core fracture shape, which verifies the reliability of the coefficient to a certain extent.

The main factors affecting the complexity of rock fractures were determined through whole-rock mineral analysis tests and triaxial mechanical experiments. As shown in Table 3, according to single-factor correlation analysis, the factors affecting the complexity of rock fractures mainly include quartz content, Young's modulus, and peak stress [27].

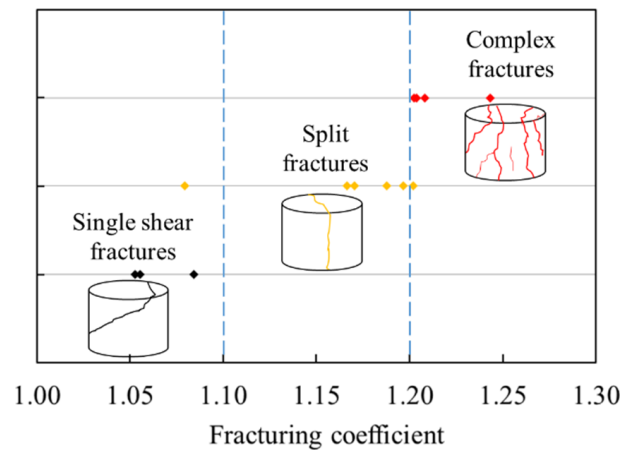


Figure 4. Core fracture morphology under different fracturing coefficients. Black dots represent single shear fractures, yellow dots represent split fractures, and red dots represent complex fractures.

Table 3. Analysis of influencing factors of rock fracture complexity.

Influencing Factor	Correlation Coefficient	Influencing Factor	Correlation Coefficient	Influencing Factor	Correlation Coefficient
Clay	0.0276	Peak stress	0.1446	Young's modulus	0.1269
Quartz	0.1071	Peak strain	0.0019	Poisson's ratio	0.0076
Feldspar	0.0004	Residual stress	0.0453	—	—
Carbonate	0.0858	Residual strain	0.0405	—	—

2.3. Evaluation of Rock Brittleness Index

Based on the above analysis, the quartz content, Young's modulus, and peak stress were selected as key indicators affecting the rock brittleness of this block, and a suitable low-permeability sandstone brittleness evaluation method for this block was established. The equation used is as follows:

$$B_{ls} = W_1 Q_n + W_2 E_n + W_3 \sigma_{pn} \quad (3)$$

where B_{ls} is the dimensionless low-permeability sandstone brittleness index; Q_n , E_n , and σ_{pn} are the normalized quartz content, Young's modulus, and peak stress, respectively; and W_1 , W_2 , and W_3 are the weight coefficients of each dimensionless parameter.

The weight coefficients of each influencing parameter were obtained by grey relational analysis; the quartz content, Young's modulus, and peak stress were 0.303, 0.358, and 0.339, respectively.

Young's modulus can be obtained from sonic logging and density logging data. Quartz mineral content can be obtained from elemental capture spectroscopy logging data. However, peak stress cannot be obtained from well log data; therefore, the approximated peak stress was used for the adjacent wells in the same block.

$$E = a \frac{\rho_r}{\Delta t_s^2} \left(\frac{3\Delta t_s^2 - 4\Delta t_p^2}{\Delta t_s^2 - \Delta t_p^2} \right) \quad (4)$$

where E is Young's modulus, MPa; a is unit conversion factor; ρ_r is the rock density, g/m^3 ; t_s is shear wave log data, $\mu\text{s}/\text{m}$; and t_p is compression wave log data, $\mu\text{s}/\text{m}$.

The brittleness index was then calculated using Equation (3). Finally, according to the calculation results, the formation with a high brittleness index was selected as the perforation location; thus, the extension position of the hydraulic fractures in the reservoir could be determined.

3. Fracture Morphology Optimization Based on Fracturing Flooding Simulation

3.1. Fracturing Flooding Mathematical Model

The following conditions were assumed in this model.

- The reservoir matrix was heterogeneous and anisotropic, with three-dimensional hexahedrons of equal horizontal thickness.
- The fracture direction was consistent with the maximum horizontal principal stress, and the fractures were homogeneous and isotropic.
- The fluid only considered the two phases of oil and water, and the oil displacement agent existed only in the water phase.
- The fluid, matrix, and fractures could be compressed to a certain extent, and the compressibility coefficient was constant.
- The reservoir was maintained at a constant temperature, and capillary imbibition was considered in the matrix.
- The bottom-hole pressure of the production well was constant; the injection rate and pressure were kept constant.
- Hydraulic fracture direction is the maximum horizontal principal stress direction, and the fracture length is constant.

The mathematical equations for the oil and water phase seepage in the matrix are as follows:

$$\frac{\partial}{\partial t}(\varphi_m \rho_\kappa S_{\kappa,m}) + \nabla \cdot (\rho_\kappa \vec{v}_{\kappa,m}) = q_{\kappa,m}^w + q_{\kappa,fm} \quad (5)$$

$$\vec{v}_{\kappa,m} = -k_m \frac{k_{r\kappa}}{\mu_\kappa} \nabla p_{\kappa,m} \quad (6)$$

where φ_m is the dimensionless reservoir matrix porosity, ρ_κ is the density of fluid κ (g/cm^3), κ denotes oil or water, $S_{\kappa,m}$ is the saturation of fluid κ in the reservoir matrix (dimensionless), $q_{\kappa,m}^w$ is the flow exchange term for fluid κ between the wellbore and reservoir matrix (m^3/d), $q_{\kappa,fm}$ is the flow exchange term for fluid κ between the wellbore and reservoir matrix (that is, the flow of fluid κ from the fracture to the reservoir matrix (m^3/d)), k_m is the absolute permeability of the reservoir matrix (mD), $k_{r\kappa}$ is the dimensionless relative permeability of fluid κ , μ_κ is the viscosity of fluid κ ($\text{mPa}\cdot\text{s}$), $p_{\kappa,m}$ is the pressure of fluid κ in the reservoir matrix (MPa), and t is the production time (s).

The mathematical equations for the flow of the oil and water phases in the fractures are as follows.

$$\frac{\partial}{\partial t}(\varphi_f \rho_\kappa S_{\kappa,f}) + \nabla \cdot (\rho_\kappa \vec{v}_{\kappa,f}) = q_{\kappa,f}^w + q_{\kappa,fm} \quad (7)$$

$$\vec{v}_{\kappa,f} = -k_f \frac{k_{r\kappa}}{\mu_\kappa} \nabla p_{\kappa,f} \quad (8)$$

where φ_f denotes the dimensionless fracture porosity, $S_{\kappa,f}$ is the saturation of fluid κ in the fracture (dimensionless), $q_{\kappa,f}^w$ is the flowrate of fluid κ from the production well to the fracture (m^3/d), $q_{\kappa,fm}$ is the flowrate of fluid κ from the reservoir matrix to the fracture (m^3/d), k_f is the absolute permeability of the fracture (mD), and $p_{\kappa,f}$ is the pressure of fluid κ in the fracture (MPa).

The stress-sensitive equations for porosity and permeability can be obtained by considering the compressibility of the fractures and matrix.

$$\begin{cases} \varphi_m = \varphi_{m0} e^{C(p_{mf} - p_0)}, \varphi_f = \varphi_{f0} e^{C_f(p_{ff} - p_0)} \\ k_m = k_{m0} e^{d(p_{mf} - p_0)}, k_f = k_{f0} e^{d_f(p_{ff} - p_0)} \end{cases} \quad (9)$$

where φ_{m0} is the dimensionless initial reservoir matrix porosity, C is the dimensionless matrix porosity compressibility, p_{mf} is the matrix pore pressure (MPa), p_0 is the initial reservoir pressure (MPa), φ_{f0} is the dimensionless initial fracture porosity, C_f is the dimensionless fracture porosity compressibility, p_{ff} is the fracture pressure (MPa), k_{m0} is the

initial permeability of the reservoir matrix (mD), d is the dimensionless matrix permeability stress sensitivity coefficient, k_{f0} is the initial permeability of the fracture (mD), and d_f is the dimensionless fracture permeability stress sensitivity coefficient.

Because the permeability in the fracture was relatively large, the capillary force was regarded as zero [29]. The matrix had a capillary pressure, which is expressed as

$$p_{of} = p_{wf}, p_{om} - p_{wm} = p_c \quad (10)$$

where p_{of} is the oil pressure in the fracture (MPa), p_{wf} is the water pressure in the fracture (MPa), p_{om} is the oil pressure in the matrix (MPa), p_{wm} is the water pressure in the matrix (MPa), and p_c is the capillary pressure in the matrix (MPa).

The distribution of the oil-displacing agent was simulated by solving the conservation equation for the oil-displacing agent in the water phase.

$$\frac{\partial}{\partial t}(\varphi_m C_s \rho_s) + \text{div}\left(\frac{C_s k_m k_{rw} \cdot \text{grad} p}{\mu_{ws}} + \varphi S_{wm} D_w^s \cdot \text{grad} C_s\right) + Q_a = Q_s \quad (11)$$

where C_s is the volume fraction of the oil-displacing agent in the water phase (%), ρ_s is the density of the oil-displacing agent (kg/m^3), μ_{ws} is the solution viscosity of the oil-displacing agent and water mixture (mPa·s), D_w^s is the dimensionless diffusion coefficient of the oil-displacing agent in the water phase, Q_a is the adsorption term of the oil-displacing agent in the pore matrix, and Q_s is the injection source term of the oil-displacing agent.

The model considered the effect of the oil displacement agent concentration on the relative permeability model, capillary force, water phase viscosity, oil-displacing agent adsorption capacity, and rock wettability, and the specific influence law was obtained from the experiment [30]. The relative permeability used as the value of the miscibility function between the two endpoints was calculated in two steps. First, the endpoints of the curves were interpolated, and the immiscibility and miscibility curves were scaled to fit these points. Finally, the relative permeability values on both curves were determined, and the final relative permeability was used as an interpolation between these two values.

The production well should satisfy the bottom-hole flow pressure to maintain a constant; thus, the Peaceman model was adopted for the inner boundary condition [31]. The oil-displacing agent at the bottom of the well was given a specific initial concentration value, and the later concentration was completely updated implicitly at the end of each time step after the oil and water phase flow rates were calculated.

$$\begin{cases} q_{\kappa,f}^w = WI_f(p_f - p_w) \\ q_{\kappa,m}^w = WI_m(p_m - p_w) \\ Q_s = q_{w,m}^w \times C_s^w \end{cases} \quad (12)$$

where WI_f is the well index in the fracture grid ($\text{m}^3/\text{d}\cdot\text{MPa}$), p_f is the pressure in the fracture (MPa), p_w is the bottom-hole flow pressure (MPa), WI_m is the well index in the matrix grid ($\text{m}^3/\text{d}\cdot\text{MPa}$), p_m is the pressure in the matrix (MPa), $q_{w,m}^w$ is the water flow exchange term between the wellbore and reservoir matrix (m^3/d), and C_s^w is a constant that represents the volume fraction of the oil-displacing agent at the bottom of the injection well (%).

The outer boundary conditions belong to the no-flow boundary category and satisfy the Neumann model.

$$\left. \frac{\partial p}{\partial n} \right|_{\Gamma} = 0 \quad (13)$$

The initial conditions of the model include initial reservoir pressure and original oil saturation.

$$\begin{cases} p(x, y, z)|_{t=0} = C_1 \\ s(x, y, z)|_{t=0} = C_2 \end{cases} \quad (14)$$

Finally, the fracturing flooding model was solved using the finite difference method.

3.2. Numerical Simulation of Fracturing Flooding

According to the typical fracturing flooding well group (well G) in the low-permeability sandstone reservoir of the fourth member of the Shengli oilfield, a numerical model was established, as shown in Figure 5, including one water injection well and four production wells. The fracture direction of the fracturing well was consistent with that of the maximum horizontal principal stress (NE45°). The half-length of the crack was 110 m, and its conductivity was 20 D·cm. The oil–water relative permeability and capillary pressure of the matrix in this model were obtained from core experiments, as shown in Figure 6, and the other reservoir geological parameters are shown in Table 4. After simulating fracturing and flooding, the water injection well injects a constant amount of liquid daily, and the production well is produced at a constant pressure.

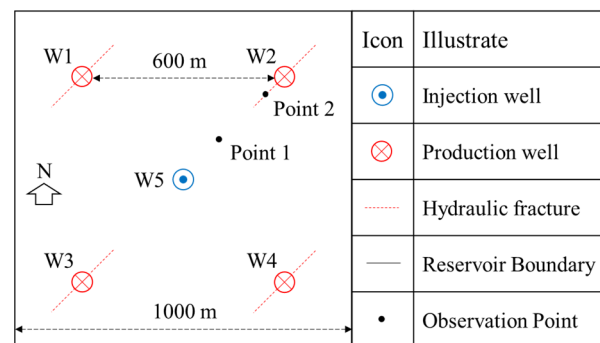


Figure 5. Schematic of fracturing flooding well group.

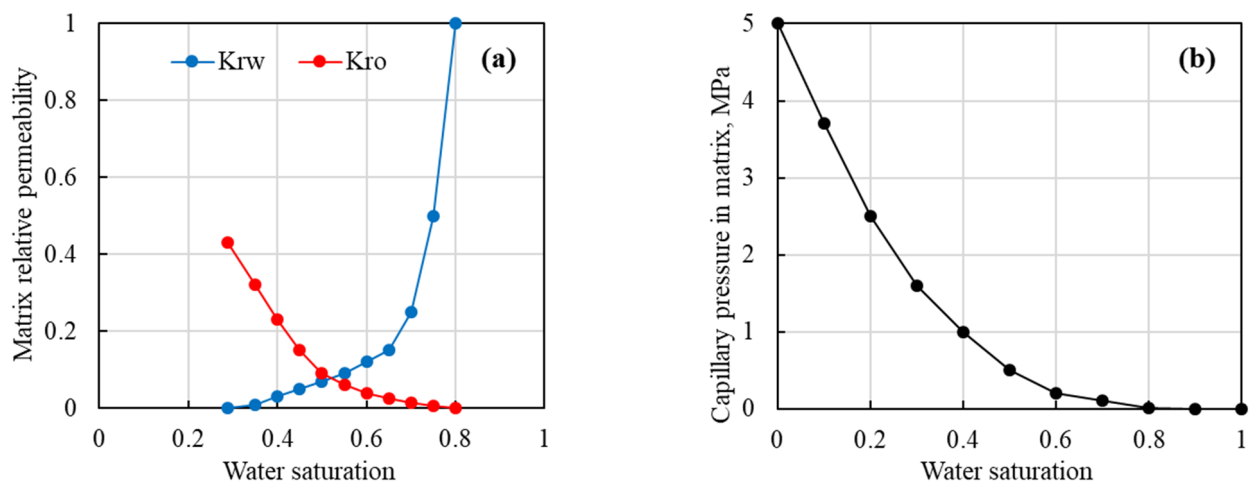


Figure 6. Matrix oil–water phase permeability (a) and capillary pressure curves (b).

Table 4. Reservoir geological parameters.

Parameters	Value	Parameters	Value
Model size (m)	1000 × 1000 × 30	Rock compression properties (MPa ⁻¹)	6.0 × 10 ⁻⁶
Surface crude oil density (g·cm ⁻³)	0.86	Formation water compressibility (MPa ⁻¹)	4.42 × 10 ⁻⁶
Surface water density (g·cm ⁻³)	1.00	Crude oil compressibility (MPa ⁻¹)	3.60 × 10 ⁻⁵
Surface crude oil viscosity (mPa·s)	21.10	Original gas oil ratio	27.40
Formation water viscosity (mPa·s)	0.46	Formation temperature (°C)	112.00
Formation crude oil volume factor	1.30	Regional formation pressure (MPa)	30.00
Matrix porosity (%)	12	Formation pressure coefficient	1.10
Matrix permeability (mD)	5	Reservoir vertical depth (m)	2900.00

To verify the model's reliability, the calculation results of this model and CMG software results were compared under the same production and injection conditions. As shown in Figure 7, the errors in the average formation pressure and cumulative production after 3 years of well group production are within 5%, indicating that the model has good reliability.

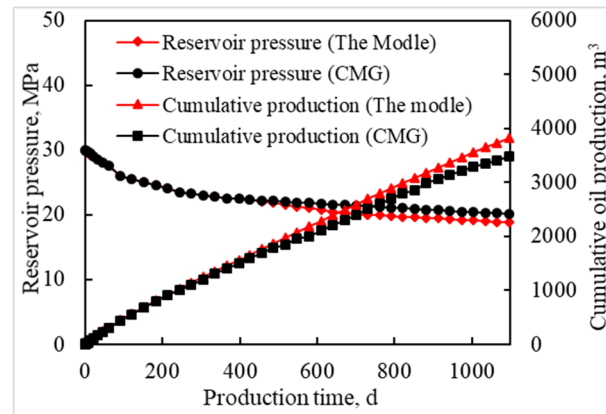


Figure 7. The calculation results of the model and CMG.

3.2.1. The Effect of Fracturing

Conventional water injection was performed in well W5 at an injection rate of $30 \text{ m}^3/\text{d}$. The production well was simulated under the conditions of no fracturing and fractures caused by fracturing, and the effect of fracturing on the production of the well group was analyzed. In Figure 5, point 1 represents the matrix and point 2 represents the fracture. The evolution process of reservoir physical properties in the production process is studied by analyzing the change rules of porosity and permeability at the two points. As shown in Figure 8, the stress sensitivity effect has a great impact on fracture permeability in the production process. The porosity and permeability of the reservoir matrix and fracture porosity have little change.

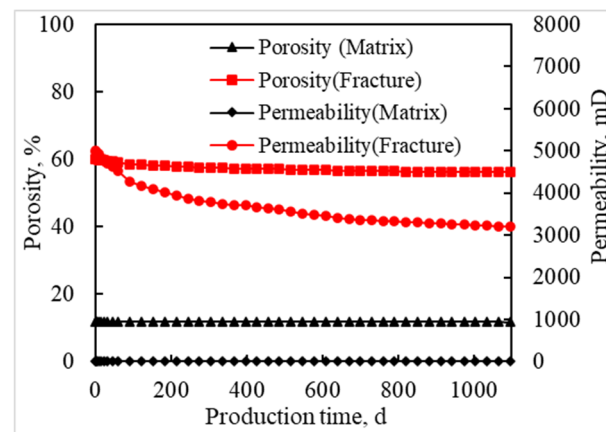


Figure 8. Evolution process of porosity and permeability.

As shown in Figure 9, using well W1 as an example, under the condition of no fracturing, the single-well productivity is low, and the initial daily oil production is only 1.58 m. After fracturing, the initial daily production of a single well increased to 8.02 m, and the multiplication ratio was 5.1. The 3-year cumulative production increased by 2066 m^3 , which shows good fracturing stimulation potential.

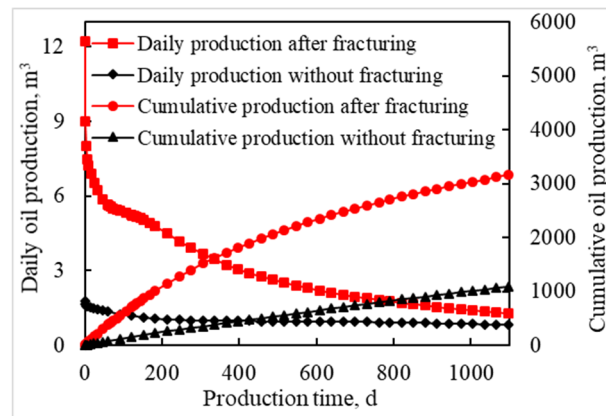


Figure 9. Production of well W1 with and without fracturing.

3.2.2. The Effect of Fracture Orientation

Well W1 was located in the minimum horizontal principal stress direction of the water injection well (W5), and well W2 was located in the maximum horizontal principal stress direction of W5. The fracture orientations of the two wells were inconsistent with the effective direction of water injection, but the other fracture parameters were the same; therefore, the production conditions were compared. As shown in Figure 10, the fracture direction of well W1 was perpendicular to the line connecting the oil injection wells. In the pressure flooding process, the water injection front advanced evenly, the water cut increased more slowly, and the initial production declined more slowly. Water injection lasted longer. The direction of the fracture in well W2 was parallel to the line connecting the oil injection well. During the water injection process, the water flooding front protruded more considerably along the dominant fracture channel, resulting in a faster rise in the water cut and rapid decline in the production of the well. Therefore, the effect of fracture orientation on the production effect of production wells should be fully considered in the process of reservoir development and well deployment.

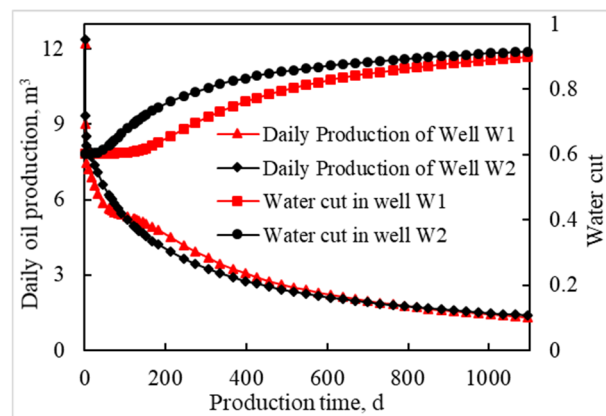


Figure 10. Production situation under different fracture orientation conditions.

3.2.3. The Effect of Oil Displacement Agent

Taking well W1 as an example, the production process of conventional water injection and the effect of the oil displacement agent addition were simulated. The mass concentration of the oil displacement agent was 0.5%, and the influence of the oil displacement agent on the production effect during the water injection process was analyzed. As shown in Figure 11, the production trend in the early stages of the two cases is the same; the single-well production decreases and the water cut increases. After 400 d of production, the oil-displacing agent reached the vicinity of the production well, the oil–water mobility

ratio increased, and the water-cut rise rate slowed down. The daily oil production was stable at approximately 3 m^3 , and the cumulative oil increase was 643.7 m^3 in 3 years.

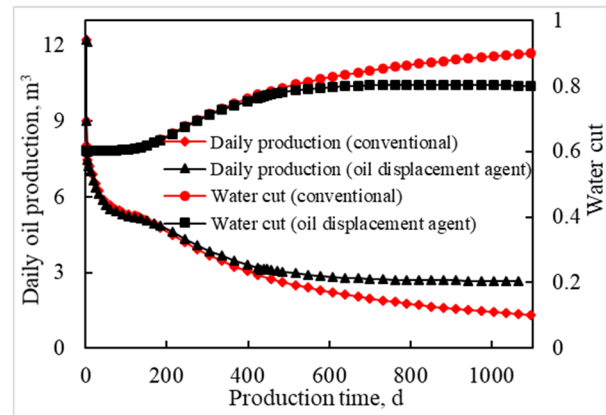


Figure 11. Influence of oil displacement agent on production efficiency.

3.2.4. Comparison between Fracturing Flooding and Conventional Fracturing

According to the fracturing flooding technology of low-permeability sandstone reservoirs in the Shengli oilfield, water was rapidly injected into the formation of well W5 at an injection rate of $0.5 \text{ m}^3/\text{min}$ (the mass concentration of the oil displacement agent was 0.5%) to supplement the formation energy. After 2 months, a total of $43,200 \text{ m}^3$ was injected. Conventional water injection with an injection rate of $30 \text{ m}^3/\text{d}$ was subsequently used, and the production well was opened for production. A comparison between the fracturing flooding process and conventional fracturing production is shown in Figure 12. The daily oil production of conventional fracturing was 8.02 m^3 , and the cumulative oil production after 3 years was 3793 m^3 . After the completion of fracturing flooding, the formation energy was sufficient, and the initial daily oil production was 27.3 m^3 . However, the production decreased rapidly in the early stages. After 180 d of fracturing flooding, the production dropped to the same level as that of conventional fracturing (4.2 m^3). In other words, the period of fracturing flooding was valid for 6 months, and after 3 years, the cumulative oil increase was 970 m^3 , and the effect of fracturing flooding was obvious.

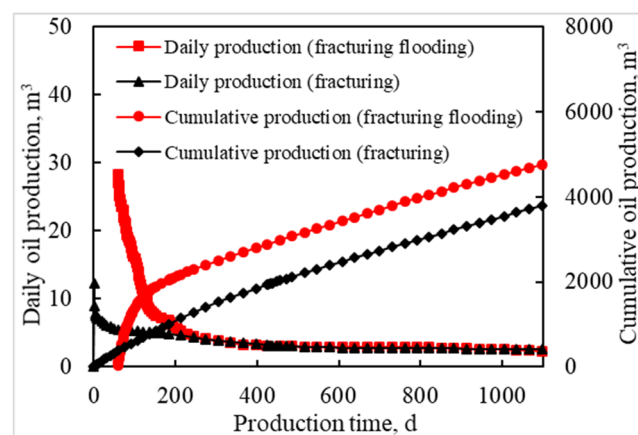


Figure 12. Comparison between fracturing flooding and conventional fracturing.

3.3. Fracture Morphology Optimization

Taking wells W1 and W2 located in different horizontal principal stress directions of injection well W5 as an example, under the condition of constant production pressure difference, the 3-year cumulative oil production was used as the index to optimize the fracture length and conductivity. As shown in Figure 13, with an increase in the fracture

half-length, the 3-year cumulative oil production of well W1 continued to increase, but the rate of increase continued to decrease. Based on the increase in production, the fracture half-length of well W1 was optimized to 90 m. The production of well W2 was more significantly affected by the fracture length. When the fracture half-length was less than 80 m, the cumulative oil production increased with the fracture length. When the fracture half-length was greater than 80 m, with a further increase in the fracture length, water channeling occurred sooner in the production well owing to the influence of the water injection front, which significantly affected the production. Therefore, the optimal fracture half-length of well W2 is 80 m.

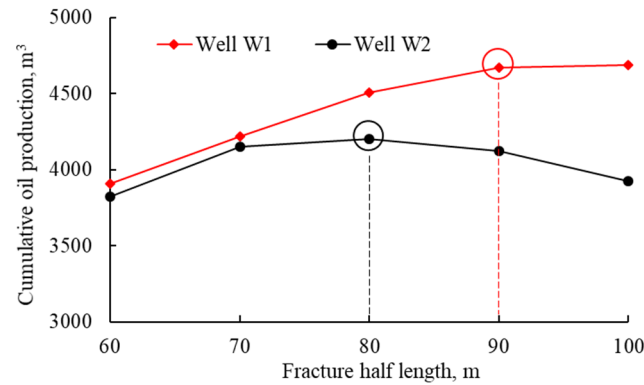


Figure 13. Fracture half-length optimization results.

Based on the optimal fracture length, the 3-year cumulative oil production under a conductivity of 15–35 D·cm was simulated. As shown in Figure 14, with an increase in conductivity, the cumulative production increases continuously but the rate of increase gradually decreases. Considering the economic benefits, the optimized fracture conductivities of wells W1 and W2 were 20 and 25 D·cm, respectively.

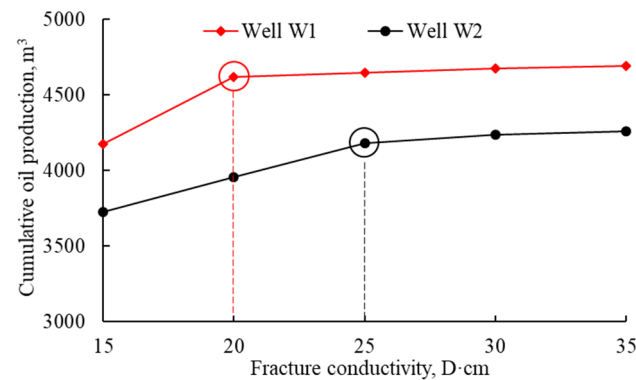


Figure 14. Fracture conductivity optimization results.

4. Field Application

Taking the low-permeability sandstone reservoir fracturing flooding well group (G well group) in the Shengli oilfield as an example, field implementation was carried out based on previous research results. According to the logging data of the well, the corresponding reservoir parameters were sorted, and a small layer with a higher brittleness index was selected as the perforation location. As shown in Figure 15, the red circle represents the preferred perforation position. According to the optimization results of the fracturing flooding numerical simulation, the half-length of the fractures in wells W1 and W4, located in the direction of the minimum horizontal principal stress of the injection well (W5), was designed to be 90 m, and their conductivity was 20 D·cm. The half-length of the fractures in wells W2 and W3, located in the direction of the maximum horizontal principal

stress of the water injection well, was designed to be 80 m, and the conductivity was 25 D·cm. The construction parameters were optimized based on the fracture parameters and implemented on-site.

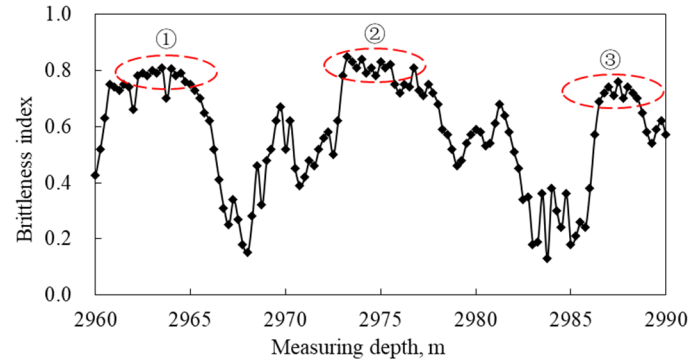


Figure 15. Perforation location optimization results. ①, ② and ③ represent three perforation positions respectively.

Considering well W1 as an example for post-fracturing analyses, well W6 is an adjacent well in the same layer as well W1, and well W6 adopts conventional methods for fracturing design and implementation. The comparison parameters are listed in Table 5. As shown in Figure 16, because the sandstone interval with a higher brittleness index is more likely to initiate fracture, the fracture pressure of well W1 at the preferred perforation location was lower, and the pumping pressure was reduced by 5–10 MPa, which effectively reduced the construction risk. According to the net pressure fitting results, the actual half-fracture length of well W1 was 87.4 m, the conductivity was 20.5 D·cm, and the errors in the design parameters were less than 3%.

Table 5. Construction parameter comparison results.

Well Name	Fracture Pressure (MPa)	Pumping Pressure (MPa)	Design Half-Fracture Length (m)	Actual Half-Fracture Length (m)	Design Conductivity (D·cm)	Actual Conductivity (D·cm)	Daily Oil Production (m ³)
W1	31.2	36~40	90	87.4	20	21.4	12.5
W6	38.5	41~50	120	116.3	30	32.8	6.9

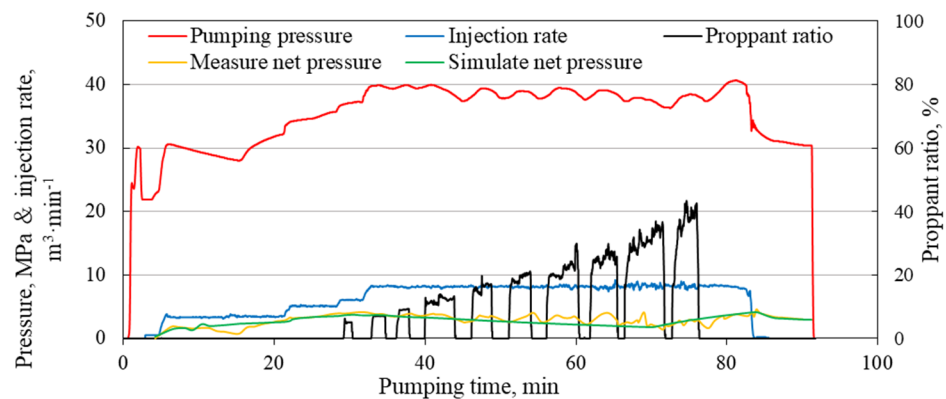


Figure 16. Construction data fitting curve.

By comparing the two wells under different fracturing parameters (Figure 17), it can be seen that the initial daily oil production of well W1 was 12.5 m³, which is 5.6 m³ higher than that of well W6, and the production of well W1 was stable for a longer time. This series of technologies were adopted by Shengli oilfield and applied to more than

20 low-permeability sandstone production wells in the Bohai Bay basin, and the average daily oil production per well increased by 3.5 m^3 , which greatly improved the fracturing stimulation effect.

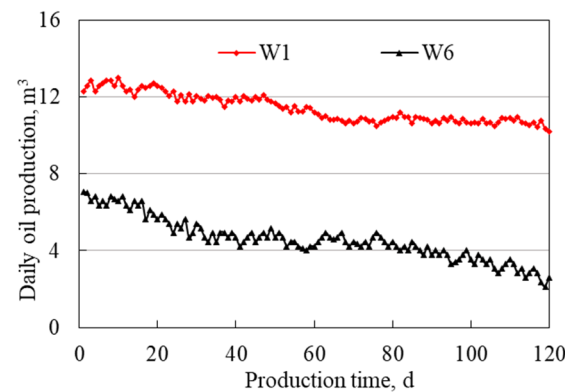


Figure 17. Daily oil production curve.

5. Conclusions

- (1) Feldspar, quartz, carbonate, and clay are the main minerals of the low-permeability sandstone in the Bohai Bay basin, with contents of 41%, 34%, 9%, and 16%, respectively. The average Young's modulus and Poisson's ratio of the rocks in the fourth member of Shahejie are 14,856 MPa and 0.254, respectively.
- (2) From the three aspects of rock mineral composition, mechanical parameters, and stress–strain characteristics, it is concluded that the main controlling factors affecting the complexity of rock fractures mainly include quartz content, Young's modulus, and peak stress. The brittleness index was evaluated, and the weight coefficients of the influencing factors were calculated as 0.303, 0.358, and 0.339, respectively.
- (3) For production wells, in the direction of minimum horizontal principal stress, the swept area of water flooding should be expanded, the fracture length should be optimized to 90 m, and the fracture conductivity should be 20 D·cm. To fracture production wells in the direction of the maximum horizontal principal stress, the advancing speed of the water injection front should be slowed down to reduce the risk of water channeling in injection-production wells. The optimized fracture length was 80 m, and the fracture conductivity was 25 D·cm.
- (4) The fracturing perforation location was optimized by analyzing the brittleness index of the target interval of the reservoir, and the fracture parameters were optimized by numerical simulation of fracturing flooding. This series of technologies was adopted by the Shengli oilfield and applied to more than 20 low-permeability sandstone production wells in the Bohai Bay basin, which increased the average daily oil production per well by 3.5 m^3 , prolonged the stable production time, and enhanced the fracturing stimulation effect to a certain extent.

Author Contributions: C.L., conceptualization, methodology, supervision, funding acquisition, writing—review and editing; L.M., methodology, validation, writing—original draft, investigation, writing—review and editing; J.G., supervision, funding acquisition; L.Z., supervision, funding acquisition; S.X., methodology, validation; B.C., supervision, funding acquisition; Y.Z., supervision, funding acquisition; H.Y., supervision, funding acquisition; Z.T., supervision, funding acquisition. All authors have read and agreed to the published version of the manuscript.

Funding: This research was funded by the National Natural Science Foundation of China (grant number 52022087), National Natural Science Foundation of China Joint Fund Project Key Support Project (grant number U21A20105), and the major project of CNOOC Beijing Research Institute: Study on multi-scale and multi-dimensional Optimization Technology of geoenvironment integration for offshore low permeability reservoir (CCL2022RCPS0361KQN).

Institutional Review Board Statement: Not applicable.

Informed Consent Statement: Not applicable.

Data Availability Statement: Data are available in the article.

Acknowledgments: All individuals included in this section have consented to the acknowledgment.

Conflicts of Interest: The authors declare no conflict of interest.

Nomenclature

D	the fractal dimension of the core end-face fracture
R	the side length of the square boxes (cm)
N	the number of square boxes containing fractures
C_p	the proportionality constant
F_c	the fracturing coefficient
α	the fracture angle ($^\circ$)
B_{ls}	the dimensionless low-permeability sandstone brittleness index
Q_n	the normalized quartz content
E_n	the normalized Young's modulus
σ_{pn}	the normalized peak stress
W_1, W_2, W_3	the weight coefficients of each dimensionless parameter
E	Young's modulus (MPa)
a	the unit conversion factor
ρ	the rock density (g/m^3)
t_s	the shear wave log data ($\mu\text{s}/\text{m}$)
t_p	the compression wave log data ($\mu\text{s}/\text{m}$)
φ_m	the dimensionless reservoir matrix porosity
ρ_κ	the density of fluid κ (g/cm^3)
κ	oil or water
$S_{\kappa,m}$	the saturation of fluid κ in the reservoir matrix
$q_{\kappa,m}^w$	the flow exchange term for fluid κ between the wellbore and reservoir matrix (m^3/d)
$q_{\kappa,fm}$	the flow exchange term for fluid κ between the wellbore and reservoir matrix—that is, the flow of fluid κ from the fracture to the reservoir matrix (m^3/d)
k_m	the absolute permeability of the reservoir matrix (mD)
$k_{r\kappa}$	the dimensionless relative permeability of fluid κ
μ_κ	the viscosity of fluid κ (mPa·s)
$p_{\kappa,m}$	the pressure of fluid κ in the reservoir matrix (MPa)
t	is the production time (s)
φ_f	the dimensionless fracture porosity
$S_{\kappa,f}$	the saturation of fluid κ in the fracture (dimensionless)
$q_{\kappa,f}^w$	the flowrate of fluid κ from the production well to the fracture (m^3/d)
$q_{\kappa,mf}$	the flowrate of fluid κ from the reservoir matrix to the fracture (m^3/d)
k_f	the absolute permeability of the fracture (mD)
$p_{\kappa,f}$	the pressure of fluid κ in the fracture (MPa)
φ_{m0}	the dimensionless initial reservoir matrix porosity
C	the dimensionless matrix porosity compressibility
p_{mt}	the matrix pore pressure (MPa)
p_0	the initial reservoir pressure (MPa)
φ_{f0}	the dimensionless initial fracture porosity
C_f	the dimensionless fracture porosity compressibility
p_{ft}	the fracture pressure (MPa)
k_{m0}	the initial permeability of the reservoir matrix (mD)
d	the dimensionless matrix permeability stress sensitivity coefficient
k_{f0}	the initial permeability of the fracture (mD)
d_f	the dimensionless fracture permeability stress sensitivity coefficient
p_{of}	the oil pressure in the fracture (MPa)

p_{wf}	the water pressure in the fracture (MPa)
p_{om}	the oil pressure in the matrix (MPa)
p_{wm}	the water pressure in the matrix (MPa)
p_c	the capillary pressure in the matrix (MPa)
C_s	the volume fraction of the oil-displacing agent in the water phase (%)
ρ_s	the density of the oil-displacing agent (kg/m^3)
μ_{ws}	the solution viscosity of the oil-displacing agent and water mixture ($\text{mPa}\cdot\text{s}$)
D_{ws}	the dimensionless diffusion coefficient of the oil-displacing agent in the water phase
Q_a	the adsorption term of the oil-displacing agent in the pore matrix
Q_s	the injection source term of the oil-displacing agent
WI_f	the well index in the fracture grid ($\text{m}^3/\text{d}\cdot\text{MPa}$)
p_f	the pressure in the fracture (MPa)
p_w	the bottom-hole flow pressure (MPa)
WI_m	the well index in the matrix grid ($\text{m}^3/\text{d}\cdot\text{MPa}$)
p_m	the pressure in the matrix (MPa)
$q_{w,m}^w$	the water flow exchange term between the wellbore and reservoir matrix (m^3/d)
C_s^w	a constant that represents the volume fraction of the oil-displacing agent at the bottom of the injection well (%)

References

1. Wu, Q.; Xu, Y.; Wang, X.Q.; Wang, T.F.; Zhang, S.L. Volume fracturing technology of unconventional reservoirs: Connotation, optimization design and implementation. *Pet. Explor. Dev.* **2012**, *39*, 352–358. [[CrossRef](#)]
2. Xu, Y.; Lei, Q.; Chen, M.; Wu, Q.; Yang, N.Y.; Weng, D.W.; Li, D.Q.; Jiang, H. Progress and development of volume stimulation techniques. *Pet. Explor. Dev.* **2018**, *45*, 874–887. [[CrossRef](#)]
3. Lei, Q.; Guan, B.S.; Cai, B.; Wang, X.; Xu, Y.; Tong, Z.; Wang, H.Y.; Fu, H.F.; Liu, Z.; Wang, Z. Technological progress and prospects of reservoir stimulation. *Pet. Explor. Dev.* **2019**, *46*, 580–587. [[CrossRef](#)]
4. Ding, B.; Xiong, C.M.; Geng, X.F.; Guan, B.S.; Pan, J.J.; Xu, J.G.; Dong, J.F.; Zhang, C.M. Characteristics and EOR mechanisms of nanofluids permeation flooding for low-permeability oil. *Pet. Explor. Dev.* **2020**, *47*, 756–764. [[CrossRef](#)]
5. He, J.G.; Wang, H.W. Design and Effect of Fracture-flooding in Class III Oil Reservoirs. *J. Southwest Pet. Univ. Sci. Technol. Ed.* **2018**, *40*, 95–104.
6. Xu, B. *Study on Mechanism and Mathematical Model of Fracturing and Percolation Enhanced Oil Recovery in Medium and Low Permeability Reservoirs: An Example in the Xingbei Development Zone of Daqing Oilfield*; Northeast Petroleum University: Daqing, China, 2019.
7. Wang, J.L.; Liu, Y.Z.; Chen, M.Q.; Liu, L.; Gao, J. Experimental study on dynamic imbibition mechanism of low permeability reservoirs. *Pet. Explor. Dev.* **2009**, *36*, 86–90.
8. Liu, H.L.; Xiong, W.; Gao, S.S.; Xue, H.; Hu, Z.M. Physical Modeling of Water-Oil Displacement in Hydraulic Fractured Horizontal Wells. *Xinjiang Pet. Geol.* **2010**, *31*, 171–173.
9. Zhang, H.N.; Chen, J.T. Insights into Energy Storage Bulk Fracturing Technology for Low-permeability Oilfields—A Case Study of Peripheral Wellblock of Jilin Oilfield. *Unconv. Oil Gas* **2015**, *2*, 55–60.
10. Wu, Z.B.; Li, L.; Yan, Y.Q. New development pattern of network fracturing and imbibition oil recovery for super-low permeability oil reservoirs. *Fault-Block Oil Gas Field* **2019**, *26*, 491–494.
11. Shi, Y.H. *Subject: Study on Fracturing Fluid's Imbibition of Chang-7 Source Based on Nuclear Magnetic Resonance*; Xi'an Shiyou University: Xi'an, China, 2018.
12. Xu, Y.H.; Meng, Y.; Shi, S.G. Design Method of Water Injection Rate for High-Pressure Water Injection in Low Permeability Reservoirs. *Inn. Mong. Petrochem. Ind.* **2021**, *47*, 118–121.
13. Lu, C.; Ma, L.; Zhang, T.; Guo, J.C.; Li, M.; Huang, B. A novel hydraulic fracturing method and case study based on proppant settlement transport model. In Proceedings of the 53rd ARMA Rock Mechanics/Geomechanics Symposium, New York, NY, USA, 23–26 June 2019.
14. Tarasov, B.; Potvin, Y. Universal criteria for rock brittleness estimation under triaxial compression. *Int. J. Rock Mech. Min. Sci.* **2013**, *59*, 57–69. [[CrossRef](#)]
15. Lu, C.; Ma, L.; Li, Z.L.; Huang, F.L.; Huang, C.H.; Yuan, H.R.; Tang, Z.B.; Guo, J.C. A Novel Hydraulic Fracturing Method Based on the Coupled CFD-DEM Numerical Simulation Study. *Appl. Sci.* **2020**, *10*, 3027. [[CrossRef](#)]
16. Sun, F.Q.; Du, S.H.; Zhao, Y.P. Fluctuation of fracturing curves indicates in-situ brittleness and reservoir fracturing characteristics in unconventional energy exploitation. *Energy* **2022**, *252*, 124043. [[CrossRef](#)]
17. Hucka, V.; Das, B. Brittleness determination of rocks by different methods. *Int. J. Rock Mech. Min. Sci. Geomech. Abstr.* **1974**, *11*, 389–392. [[CrossRef](#)]
18. Jarvie, D.M.; Hill, R.J.; Ruble, T.E. Unconventional shale-gas systems: The Mississippian Barnett Shale of north-central Texas as one model for thermogenic shale-gas assessment. *AAPG Bull.* **2007**, *91*, 475–499. [[CrossRef](#)]

19. Rickman, R.; Mullen, M.J.; Petre, J.E.; Grieser, W.V.; Kundert, D. A practical use of shale petrophysics for stimulation design optimization: All shale plays are not clones of the Barnett Shale. In Proceedings of the SPE Annual Technical Conference and Exhibition, Denver, CO, USA, 21–24 September 2008.
20. Liu, Z.S.; Sun, Z.D. New brittleness indexes and their application in shale/clay gas reservoir prediction. *Pet. Explor. Dev.* **2015**, *42*, 117–124. [[CrossRef](#)]
21. Quinn, J.B.; Quinn, D.G. Indentation brittleness of ceramics: A fresh approach. *J. Mater. Sci.* **1997**, *32*, 4331–4346. [[CrossRef](#)]
22. Xiao, Y.; Guo, J.C. Optimization of Fracturing Parameters for Low Permeability and Heterogeneous Reservoir Production well. *Sci. Technol. Eng.* **2012**, *12*, 9019–9022.
23. Xu, C.C.; Chen, C.H.; Wang, B.; Wu, Y.H.; Peng, C.J. Fracture parameter optimization of network fracturing for horizontal well in low permeability and low-permeability oil reservoir. *Fault-Block Oil Gas Field* **2014**, *21*, 823–827.
24. Lei, Q.; Weng, D.W.; Guan, B.S.; Mu, L.J.; Xu, Y.; Wang, Z.; Guo, Y.; Li, S. A novel approach of stimulation based on fracture controlling optimization and design. *Pet. Explor. Dev.* **2020**, *47*, 1–8.
25. Harimi, B.; Masihi, M.; Mirzaei-Paiaman, A.; Hamidpour, E. Experimental study of dynamic imbibition during water flooding of naturally fractured reservoirs. *J. Pet. Sci. Eng.* **2018**, *174*, 1–13. [[CrossRef](#)]
26. Lucas, M.; Mohsen, T.; Ke, X.; Miguel, M.; Du, Y.J.; Matthew, B. Surfactant flooding in oil-wet micromodels with high permeability fractures. *Fuel* **2019**, *241*, 1117–1128.
27. Lu, C.; Ma, L.; Guo, J.C.; Li, X.Y.; Zheng, Y.C.; Ren, Y.; Yin, C.B.; Li, J.F.; Zhou, G.Q.; Wang, J.D.; et al. Novel Method and Case Study of a Deep Shale Fracability Evaluation Based on the Brittleness Index. *Energy Explor. Exploit.* **2021**, *40*, 1–18. [[CrossRef](#)]
28. He, T. *Research on Compressibility Evaluation of Low-Permeability Sandstone Reservoirs in the Second Member of Kong 2 Member in Dagang Oilfield*; Southwest Petroleum University: Chengdu, China, 2016.
29. Xu, S.Q.; Ren, G.T.; Younis, R.M.; Feng, Q.H. Revisiting field estimates for carbon dioxide storage in depleted shale gas reservoirs: The role of geomechanics. *Int. J. Greenh. Gas Control* **2021**, *105*, 103222. [[CrossRef](#)]
30. Wang, J.; Liu, H.Q.; Xia, J.; Liu, Y.T.; Hong, C.; Meng, Q.B.; Gao, Y. Mechanism simulation of oil displacement by imbibition in fractured reservoirs. *Pet. Explor. Dev.* **2017**, *44*, 761–770. [[CrossRef](#)]
31. Xu, S.Q.; Guo, J.C.; Feng, Q.H.; Ren, G.T.; Li, Y.Y.; Wang, S. Optimization of hydraulic fracturing treatment parameters to maximize economic benefit in tight oil. *Fuel* **2022**, *329*, 125329. [[CrossRef](#)]

Disclaimer/Publisher’s Note: The statements, opinions and data contained in all publications are solely those of the individual author(s) and contributor(s) and not of MDPI and/or the editor(s). MDPI and/or the editor(s) disclaim responsibility for any injury to people or property resulting from any ideas, methods, instructions or products referred to in the content.